INTERNATIONAL JOURNAL OF
COASTAL & OFFSHORE ENGINEERING
IJCOE Vol.3 /No. 4 /Winter 2018 (45-55)

Available online at: http://ijcoe.org/browse.php?a_code=A-10-183-1&sid=1&slc_lang=en

Study of Flow Characteristics around a Near-Wall Circular Cylinder Subjected to a Steady Cross-Flow

Mohammad Amin Salehi[1], Said Mazaheri[2*], Mohammad Hossein Kazeminezhad[3]

[1] *Ocean Engineering & Technology, Iranian National Institute for Oceanography and Atmospheric Science, Tehran, Iran, mascivil9@gmail.com*
[2] [*] *Corresponding Author: Ocean Engineering & Technology, Iranian National Institute for Oceanography and Atmospheric Science, Tehran, Iran, said.mazaheri@inio.ac.ir*
[3] *Ocean Engineering & Technology, Iranian National Institute for Oceanography and Atmospheric Science, Tehran, Iran, mkazeminezhad@inio.ac.ir*

ARTICLE INFO

Article History:
Received: 7 Jan. 2018
Accepted: 6 Mar. 2018

Keywords:
pressure distribution
force coefficients
separation angle
stagnation angle
vortex shedding suppression

ABSTRACT

Three-dimensional RANS simulations are employed numerically to study flow characteristics around a near-wall circular cylinder for varying gap-to-diameter (G/D) ratios (Where G is the gap between the cylinder and the wall and D is the cylinder diameter) and at Reynolds numbers from 100 to 3900. Pressure distribution around the circular cylinder, base pressure magnitude, separation and stagnation angles, force coefficients and Strouhal numbers were calculated and compared for all of the cases. Inception of vortex shedding can be seen when a sudden decrease in the maximum of positive pressure coefficient occurs. Vortex shedding mechanism and possibility of suppression further investigated via comparison of swirling strength in upper and lower vortex regions through parameter Λ, which signifies vortical activity and balance with respect to the wake center-line and also the flow type parameter, λ, representing the extensional strain dominance in the wake flow and gap flow. Vortex shedding suppression observed for the cases with the high unbalance vorticity content in the vortex regions, namely for $\Lambda \geq 2$.

1. Introduction

Marine pipelines are extensively used to transport oil and gas products between offshore and onshore especially in shallow to deep waters. Pipeline free spans can be formed as a result of local scour beneath pipeline or irregularity of seabed. Vortex shedding phenomenon on a free span pipeline results in fluctuations in hydrodynamic forces acting on it. Vortex induced vibration of a cylinder subjected to steady flow is highly influenced by fluctuating lift fluid forces, damages the pipeline structure and the junctions due to fatigue. To ensure avoiding such harmful effect on the pipelines, managing the occurrence of vortex shedding is attainable through realizing the characteristics of flow around a circular cylinder near a plane boundary.

Many researchers focused on the pressure distribution and force components around a circular cylinder to describe the gap flow and wake flow characteristics. Batham [1] measured mean and fluctuating pressure distributions around a circular cylinder with smooth and rough surfaces at Reynolds number range of 1.11×10^5 to 2.35×10^5 under uniform and turbulent streams. It had been found that the introduction of free-stream turbulence at this range of Reynolds number suppresses the vortex shedding on the smooth cylinder due to three-dimensionality and small axial correlations at separation and also increases the pressure downstream of the separation point. Pressure distribution around smooth and rough cylinders found to be different for uniform incident flows, unlike the Pressure distribution pattern around smooth and rough cylinders under turbulent flows, which was observed to be similar. It can be concluded that the pressure field patterns have been largely influenced by the processes of boundary layer and shear layer transition. Bearman and Zdravkovic [2] experimentally investigated flow around a circular cylinder at various heights above a plane boundary experimentally and found out that flow around a circular cylinder near plane boundary depends on cylinder Reynolds number, gap ratio (G/D) and characteristics of the boundary layer. Distributions of mean pressure around the cylinder and along the plate were measured at a Reynolds number, based on the cylinder diameter, of 4.5×10^5. Spectral analysis of hot-wire signals

demonstrated that regular vortex shedding was suppressed for all gaps less than about 0.3 cylinder diameters and for gaps greater than 0.3 the Strouhal number was found to be remarkably constant. Zdravkovic [3] measured the lift and drag forces on circular cylinders fitted with end plates in a wind tunnel. The gap between the cylinder and the wall, G, the thickness of the turbulent boundary layer along the wall, δ, and Re were varied in the following ranges: $0 < G/D < 2$, $12 < \delta/D < 0.97$ and $4.8 \times l0^4 < Re < 3 \times l0^5$. The lift and drag coefficients were presented in terms of a new variable G/δ. It was found that the lift coefficient is governed by the gap-to-diameter ratio G/D while the drag coefficient is dominated by the ratio of gap to thickness of the boundary layer, G/δ. Buresti and Lanciotti [4] measured mean and fluctuating forces on a circular cylinder near a plane surface in cross-flow submerged in three different types of boundary layer on the plane, at Reynolds number range of 0.86 to 2.77×10^5 and for various gap distances from 0 to 1.5. They found that vortex shedding persistence and suppression, regardless of boundary layer thickness on the plane, is a coherent feature of the flow unless the vertical velocity gradient becomes excessive. Generally, The critical gap, at which the vortex shedding ceases, decreases with increasing the boundary layer thickness but it may become larger in thicker boundary layers if the velocity gradient is greater than a limit value. Effects of other parameters like bed proximity, boundary layer thickness, Reynolds number and separation angles on vortex shedding state has been investigated in other studies.

Oner et al. [5] used particle image velocimetry (PIV) technique to measure the velocity field in a steady, two-dimensional, turbulent flow around a horizontal circular cylinder near a plane boundary. They presented the results for velocity profiles, streamlines and iso-vorticity contours for seven different gap ratios and Reynolds numbers of 840, 4150 and 9500. They illustrated some of the near wall flow field parameters around the circular cylinder through a definition sketch, Fig 1. Where D is the cylinder diameter, u_0 is the free-stream velocity, δ is the boundary layer thickness, θ_s is the stagnation angle, θ_{sep} is the separation angle and G is the gap distance. The four regions of disturbed flow around a circular cylinder near a plane boundary have been illustrated by a, b, c and d labels. Region d signifies the wake region.

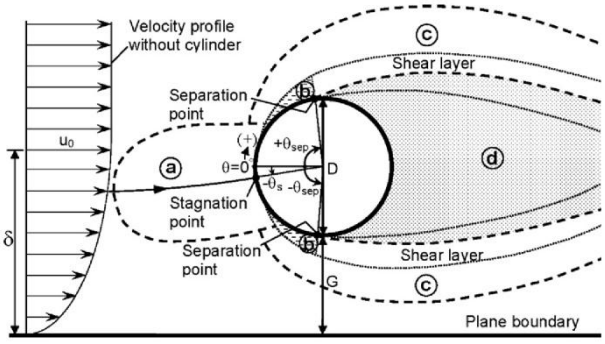

Fig. 1. Definition of near wall flow field parameters around circular cylinder, Oner et al. (2008)

Their results showed that the variations of the parameters such as separation angle, stagnation angle and Strouhal number for $G/D \geq 0.3$ and also the wall proximity effect on the flow becomes insignificant for $G/D \geq 1$. Experiments conducted by Lei et al. [6] investigated the hydrodynamic forces and vortex shedding of a circular cylinder in different boundary layers at Reynolds number range of 1.3×10^4 to 1.45×10^4. They suggested a quantitative method for identifying the vortex shedding suppression and observed that the critical gap ratio of the inception of vortex shedding suppression decreases as the thickness of boundary layer increases. Price et al. [7] visualized the flow around a circular cylinder near a plane wall for $1200 < Re < 4960$ and $0 < G/D < 2$ and categorized the flow to four distinct regions. They observed that for very small gaps ($G/D \leq 0.125$), despite the gap flow is suppressed or extremely weak, there's a periodicity attributed to the outer shear layer. They concluded that for the small gap ratio region ($0.125 < G/D < 0.5$), the pairing between the inner shear layer and the wall boundary layer is more pronounced. At the intermediate gap ratios ($0.5 < G/D < 0.75$), the onset of vortex shedding occurs and for large gap ratios ($G/D > 1$), no separation of wall boundary layer appears either upstream or downstream of the cylinder.

Wang and Tan [8] experimentally studied the flow characteristics in the near wake of a circular cylinder near a plane wall at the Reynolds number of 1.2×10^4 and for various gap ratios from 0.1 to 1. Results showed that for the gap ratio $G/D \geq 0.3$, the flow is characterized by the periodic, Karman-like vortex shedding from the upper and lower sides of the cylinder, while for small and intermediate gap ratios ($G/D \leq 0.6$), the wake flow develops a distinct asymmetry about the cylinder centerline; however, some flow quantities, such as the Strouhal number and the convection velocity of the shed vortex, keep roughly constant and virtually independent of G/D. Lin et al [9] investigated the flow characteristics in the near wake of a circular cylinder near a plane boundary experimentally at the Reynolds number range of 7.8×10^2 to 1.15×10^4 and for various gap heights (G)

from 0 to 4. Wake and gap flow characteristics inspected and it has been observed that for G/D < 0.5 A recirculating eddy is formed on the plane boundary upstream of the circular cylinder and its size increases with the decrease in gap ratio. This eddy deflects a part of the upstream fluid over the top surface of the circular cylinder and reduces the flow through the gap. For gap ratios between 0.1 and 0.3, the gap flow shows the wall-jet characteristics and a formula for recirculation zone border was presented based on the maximum value of horizontal velocity and its corresponding location.

Great efforts are made by many researchers to describe the vortex shedding and suppression mechanism and its subsequent influence on the wake flow and gap flow in the presence of the wall. The assessment of the vorticity dynamics to inspect flow unsteadiness and the instability mechanism to investigate the vortex induced instability is made by Dipankar and Sengupta [10] as they studied how lift and drag coefficients are affected by the gap ratios of G/D=0.5, G/D=1.5 and Re=1200. They concluded that the vortex induced instability occurs due to mutual interaction of vorticity field from the plane wall boundary layer and the vortices created on the cylinder surface that are shed afterwards. They considered the presence of the plane wall as a source of perturbation for the flow past the cylinder and vice versa, and observed large spatio-temporal growth of the disturbance field during wall and cylinder interactions. Physics of flow in the presence of the wall including the shear layer transition, stretching, breakdown and turbulence generation investigated by Sarkar and Sarkar [11] for a Reynolds number of 1440. They employed large-eddy simulations to assess the modifications of wake dynamics and turbulence characteristics behind a circular cylinder placed near a wall for different gap-to-diameter (G/D) ratios. They noticed that the suppression of vortex shedding and stretching of the shear layers occur due to the strong coupling between inner shear layer and approaching boundary layer while the inner shear layer is submerged inside the boundary layer ($G \leq \delta$). He et al. [12] through PIV experiments studied the dynamics of vortical structures in flow over a circular cylinder in the vicinity of a flat plate for various gap ratios ($0 < G/D < 3$) and at Re=1072. They classified the entire region of G/D into five sub-regions based on gap ratios. They observed that for G/D=0 and 0.25 the lower shear layer from the cylinder is inhibited or completely suppressed, while no distinguished peak on velocity can be detected which indicates the cease of vortex shedding process.

As noticed through reviewing the type of studies focused on the wake dynamics and vortex shedding phenomenon, still considerable uncertainties and questions remained on the mechanism of vortex shedding such as; the inception, the continuation and the suppression of vortex shedding. For instance, as the vortex shedding depends on flow regime, geometry, boundary layer characteristics and other factors, still there is no clear understanding that which one mostly influences the stability or suppression of vortex shedding. In this study, three-dimensional flow around a circular cylinder far from and near the plane boundary has been simulated numerically using Open source CFD codes of OpenFOAM. Pressure distribution around the circular cylinder, base pressure magnitude, separation and stagnation angles, force coefficients and Strouhal numbers were calculated and compared for all of the cases. Additionally, detailed velocity and vorticity fields in the wake have been discussed through parameters like Q-criterion, normalized spanwise vorticity and the flow type parameter to scrutinize the wake flow and the possibility of vortex shedding occurrence. At the end, a quantitative method in terms of parameter Λ, the ratio of swirling strength of the upper vortex sheet to the lower one, has been introduced to detect the occurrence of vortex shedding suppression.

2. Governing Equations

Time averaged Navier-Stokes equations including continuity equation are the governing equations for incompressible fluid flow:

$$\frac{\partial u_i}{\partial x_i} = 0 \tag{1}$$

Momentum equation 2 divided by ρ:

$$\rho\left(\frac{\partial u_i}{\partial t} + u_j \frac{\partial u_i}{\partial x_i}\right) = B_i - \frac{\partial p}{\partial x_i} + \mu \frac{\partial^2 u_i}{\partial x_j \partial x_j} + \frac{\partial}{\partial xj}\left(-\rho \overline{u_i' u_j'}\right) \tag{2}$$

$$\frac{\partial u_i}{\partial t} + u_j \frac{\partial u_i}{\partial x_i} = -\frac{1}{\rho}\frac{\partial p}{\partial x_i} + \nu \frac{\partial}{\partial x_j}\left[\frac{\partial u_i}{\partial x_j} + \frac{\partial u_j}{\partial x_i}\right] - \frac{\partial \overline{u_i' u_j'}}{\partial xj} \tag{3}$$

The Reynolds stress tensor approximated by Boussinesq model:

$$\overline{\partial u_i' u_j'} = \nu_t \left(\frac{\partial u_i}{\partial x_j} + \frac{\partial u_j}{\partial x_i}\right) - \frac{2}{3} k \delta_{ij} \tag{3}$$

Where u, p, ρ, υ, B and τ are the velocity, pressure, density, kinematics viscosity, body forces and Reynolds stress, respectively. K-ω SST, a two-equation eddy-viscosity turbulence model has been employed to close the system of equations. K-ω SST, presented by Menter [13] is a variant of the standard k–ω model which Combines the original Wilcox k-ω model for use near walls and the standard k–ε model away from walls using a blending function, F1, and the eddy viscosity formulation is modified to account for the transport effects of the principle turbulent shear stress. This turbulence model solves one transport equation for the turbulent kinetic energy, k, and one transport equation for the dissipation per unit

kinetic energy, ω, also regarded as a turbulent frequency scale.

The original K-ω equations, multiplied by F_1 and the transformed k–ε equations multiplied by $(1-F_1)$, have been added together to comprise the new SST model equations including the turbulence kinetic energy, equation 5 and the specific dissipation rate, equation 6:

$$\frac{\partial(\rho k)}{\partial t}+\frac{\partial(u_j k)}{\partial x_j}= P-\beta^*\rho k\omega+\frac{\partial}{\partial x_j}\left((\mu+\sigma_k\mu_t)\frac{\partial k}{\partial x_j}\right) \quad (5)$$

$$\frac{\partial(\rho\omega)}{\partial t}+\frac{\partial(u_j\omega)}{\partial x_j}=\frac{\gamma}{\nu_T}P-\beta\rho\omega^2 +\frac{\partial}{\partial x_j}\left((\mu+\sigma_\omega\mu_T)\frac{\partial\omega}{\partial x_j}\right)+2(1-F_1)\sigma_{\omega2}\frac{\rho}{\omega}\frac{\partial k}{\partial x_i}\frac{\partial\omega}{\partial x_i} \quad (6)$$

The closure coefficients and auxiliary relations such as production of k, P, and kinematic eddy viscosity, υ_t, are determined as follow, equations 7 and 8:

$$P=\min\left(\tau_{ij}\frac{\partial u_i}{\partial x_j},10\beta^*k\omega\right) \quad (7)$$

$$F_1=\tanh\left(\arg_1^4\right)= \tanh\left\{\left\{\min\left[\max\left(\frac{\sqrt{k}}{\beta^*\omega y},\frac{500\nu}{y^2\omega}\right),\frac{4\sigma_{\omega2}k}{CD_{k\omega}y^2}\right]\right\}^4\right\} \quad (8)$$

$$\alpha_1=\frac{5}{9},\quad \alpha_2=0.44,\quad \beta_1=0.075,\quad \beta_2=0.0828,\quad \beta=\frac{9}{100},$$
$$\sigma_{k1}=0.85,\quad \sigma_{k2}=1,\quad \sigma_{\omega1}=0.5,\quad \sigma_{\omega2}=0.856$$

Where y is the distance to the next surface, Ω is the vorticity tensor and CD_{kw} is the positive portion of the cross diffusion term.

3. Computational meshing

In order to select the proper mesh within the computational domain, sensitivity analysis is performed for different meshes inside subdomain 1 around the cylinder in different cases. Computational domain size and the location of subdomain 1 for the case of G/D=1 and inlet uniform velocity of 0.039 m/s, are shown in Fig. 2. Characteristics of the different computational meshes used are presented in Table 1.

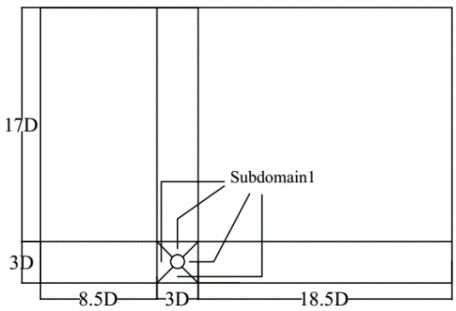

Fig. 2. Computational domain details for G/D=1

Table 1. Characteristics of different meshes used

Mesh name	Max. Δx in subdomain1	Max. Δy in subdomain1	Number of meshes per diameter in horizontal direction	Number of meshes per diameter in vertical direction
Mesh 1	0.0075	0.0075	40	40
Mesh 2	0.006	0.006	50	50
Mesh 3	0.01	0.01	30	30

According to the comparison of time-averaged velocity profiles for different mesh resolutions presented in Fig. 3, in which close results are observed, the mesh resolution 1 is selected as the optimum mesh of the computational domain used in the case of Re=3900 and G/D=1.

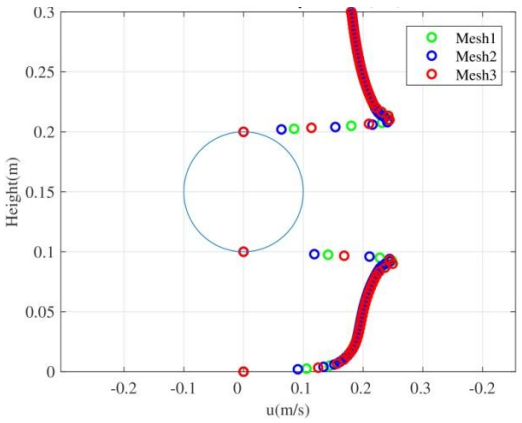

Fig. 3. Time-averaged horizontal velocity profiles for different mesh resolutions applied on subdomain 1, for Re=3900 and G/D=1

4. Near-wall treatment and free-stream initial conditions for turbulent Re=3900 cases at OpenFOAM

For Re=3900 cases turbulence has been modeled by K-ω SST turbulence model. For initial free-stream conditions, the turbulence kinetic energy, k, the turbulence specific dissipation, ω, the kinematic eddy viscosity, ν_t , and the turbulence length scale, L, can be estimated by equations 9, 10, 11 and 12 respectively.

$$k=\frac{3}{2}\left(I\left|u_{ref}\right|\right)^2 \quad (9)$$

$$\omega = k^{0.5} / c_\mu L \quad (10)$$

$$\nu_t = \sqrt{3/2} u_{ref} IL \quad (11)$$

$$L = 0.07 D_h = 0.07 D \quad (12)$$

Where I is the turbulence intensity, u_{ref} is the reference velocity, D_h is hydraulic diameter equal to cylinder diameter, D, and c_μ is a constant equal to 0.09. Depending on the dimensionless wall distance unit y^+ value, which is considered equal to 30 in all cases in order to utilize wall functions, k, ω and ν_t wall boundary conditions determined as equations 13 to 17.

$k_{wall} = kqrwallfunction = k$, acts as a zero gradient condition (13)

$$\omega_{wall} = omegawallfunction = \sqrt{\omega_{vis}^2 + \omega_{\log}^2} \quad (14)$$

$$\omega_{vis} = 6\nu / \beta_1 y^2 \quad (15)$$

$$\omega_{\log} = \sqrt{k} / \sqrt[4]{\beta^*}\kappa y \quad (16)$$

$$\nu_{twall} = nutUSpaldingwallfunction = (u_\tau)^2 / (\partial u / \partial n) - \nu \quad (17)$$

Where ω_{vis} and ω_{log} are respectively the omega values at the viscous sub-layer and logarithmic regions, β=0.075, u_τ is the friction velocity, κ is the Von Karman constant and y is the distance to the first cell center normal to the wall. Kqrwallfunction, omegawallfunction and nutUSpaldingwallfunction are the wall functions used by OpenFOAM to consider the boundary conditions on the wall. The boundary layer thickness and mesh dimension closest to the wall at y^+=30 are computed as equations 18 to 23.

$$\mathrm{Re}_x = ux / \nu \quad (18)$$

$\delta = 0.382x / \mathrm{Re}_x^{1/5}$, based on Schlichting empirical equation [14] (19)

$c_f = \left[2\log(\mathrm{Re}_x) - 0.65\right]^{-2/3}$, based on Schlichting [14] for $\mathrm{Re}_x \le 10^9$ (20)

$$\tau_\omega = \frac{1}{2}\rho c_f u_{freestream}^2 \quad (21)$$

$$u_\tau = \sqrt{\tau_\omega / \rho} \quad (22)$$

$$\Delta = y = \nu y^+ / u_\tau \quad (23)$$

Where δ is the boundary layer thickness, c_f is the skin friction coefficient, τ_ω is the wall shear stress and Δ is the dimension of the cells adjacent to the wall.

5. Model validation

Comparison of simulation results for flow around a circular cylinder far from plane boundary at Re=100, including average drag coefficient, positive maximum value of lift coefficient and Strouhal number were considered and compared with those obtained by Cao and Wan [15] and showed good agreement according to Table 2. Also the computational velocity fields from the present simulations are compared with the experimental results obtained from PIV measurements of Oner et al. [5] at Re=9500 for further validation of the numerical model, which can be seen in Fig. 4.

Table 2. Comparison of C_d, C_l(max) and S_t parameters at Re=100

	C_d	C_l (max)	S_t
Present study	1.3918	0.3229	0.1613
Cao and Wan [5]	1.3932	0.3347	0.168

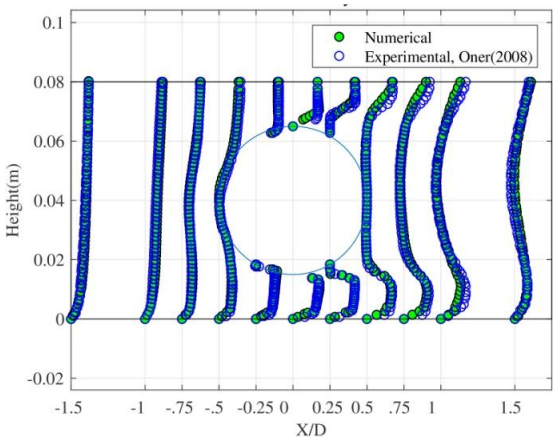

Fig. 4.comparison of horizontal velocity profiles of present numerical simulation and experimental study of Oner et. al [5] for G/D=0.3 and Re=9500

6. Results and Discussion

Time-averaged pressure distribution around a circular cylinder represented by pressure coefficient and separation points for all cases, cylinder far from and near the wall, have been presented in Figs. 5 to 8. It is seen that bell-shaped pressure coefficient distribution pattern includes a smaller section of positive pressure coefficient in front of cylinder and a bigger section of negative pressure coefficient around the other parts of the cylinder perimeter. In all cases, far from and near the wall, the symmetry of pressure coefficient around the stagnation point has been observed. Investigation of pressure coefficient around the cylinder shows that by reducing gap ratio, G/D, higher lift force pushes the cylinder upward. The amount of lift increase is less pronounced when vortex shedding is suppressed or boundary layer is thicker. By increasing G/D, positive and negative values of pressure coefficients around the cylinder are decreased, hence mean lift force on the cylinder decreases too. In high inference between the cylinder and the wall, i.e. smaller G/D, and when boundary layers around the cylinder and the wall overlap fittingly, the maximum of positive pressure coefficient increases and moves downstream.

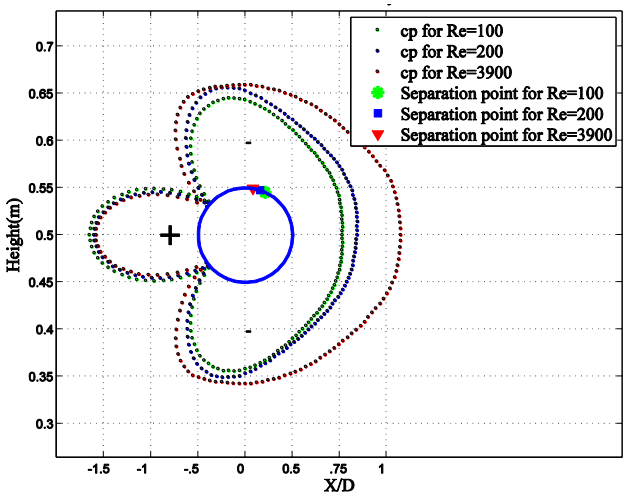

Fig. 5. Pressure coefficient distribution around circular cylinder at G/D=∞, for Re=100,200,3900

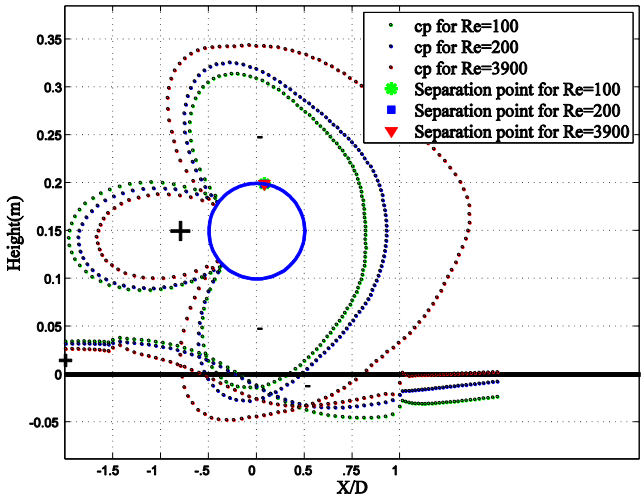

Fig. 6. Pressure coefficient distribution around circular cylinder at G/D=1, for Re=100,200,3900

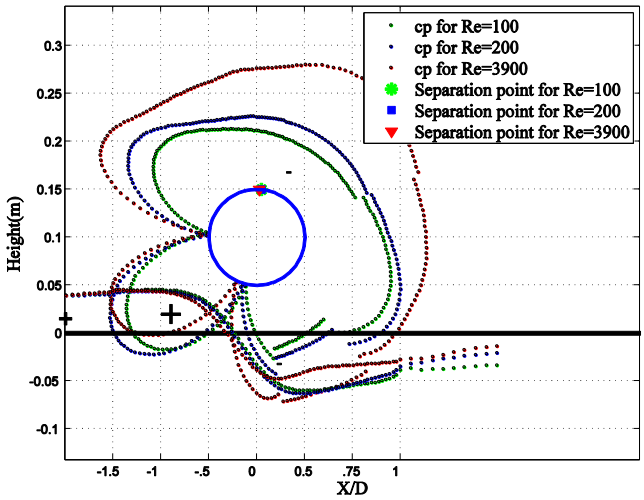

Fig. 7. Pressure coefficient distribution around circular cylinder at G/D=0.5, for Re=100,200,3900

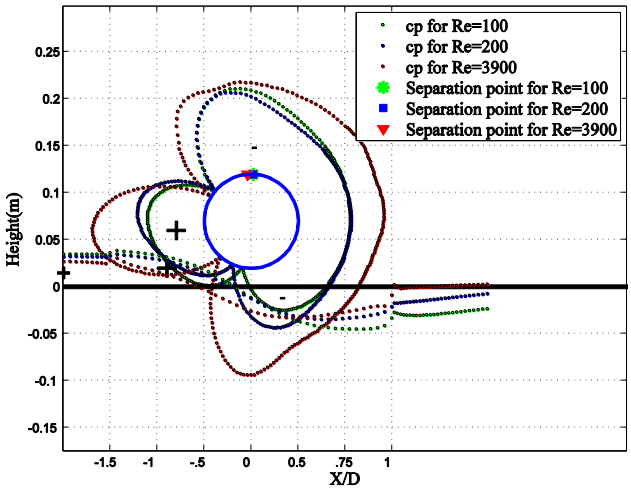

Fig. 8. Pressure coefficient distribution around circular cylinder at G/D=0.2, for Re=100,200,3900

Tables 2,3 and 4 present the results of 3-D computations including hydrodynamic drag, C_d(mean) and lift coefficients, C_l(rms), Strouhal number (st), gap to boundary layer thickness ratio (G/δ), Separation angle, Stagnation angle and base pressure, Cpb, for different gap ratios and Re=100, 200 and 3900. It has been observed that for the range of about $G/\delta < 0.55$ there is a high possibility of vortex shedding suppression. The thickness of the boundary layer, δ, can be determined by measuring the velocity profile of the boundary layer at the cylinder location.

Based on Figs. 6, 7 ,8 and 9, it can be observed that upper separation point moves counter-clockwise by increasing Reynolds number (decrease in separation angle, θ_s), in a fixed gap ratio. Also in a fixed Reynolds number, upper separation point moves upward by decreasing G/D (decrease in separation angle, θ_s). Upward displacement of upper separation point by approaching the wall, can be described by the growing stream-wise pressure gradient induced by the gap flow. Separation occurs when skin friction vanishes, where velocity gradient at the wall becomes zero. The effect of the boundary layer on the pressure distribution can be attributed to the existence of the velocity gradient in the boundary layer. Drag coefficient consists of friction drag and form (pressure) drag and major fluctuations of drag force around circular cylinder relates to form drag in a distinct flow regime. When drag coefficient, a function of pressure distribution, rapidly decreases, it can be deduced that friction drag increases with respect to form drag and velocity gradient reaches its maximum value, hence separation of boundary layer does not proceed, i.e. vortex shedding suppression occurs.

Stagnation point is the corresponding point on the cylinder surface to the maximum of positive pressure coefficient. It is shown that stagnation point moves toward wall by increasing Reynolds number (decrease in stagnation angle).

According to tables 2 to 4, Mean drag coefficient, C_d(mean) generally increases with increasing Gap ratio, G/D. But from G/D=1 to G/D=∞, considering the ratio of gap distance to cylinder boundary layer thickness, G/δ, reduction in drag coefficient observed, which is the result of the cylinder exit from the influence zone of plane wall`s boundary layer. Fig. 9 shows the variation of C_d(mean) for all cases. Oscillating lift coefficient, represented by C_l(rms), root mean square of lift coefficient, in Re=100, where boundary layer is thicker, shows bigger value near the wall. While for Re=3900, where boundary layer is thinner, C_l(rms) decreases when cylinder approaches the wall. Increase of C_l(rms) near the wall in thick boundary layer can be explained by increase of the lift coefficient near the wall, as a result of the perturbance of reverse pressure gradient above and below the cylinder which makes the positive fluctuations of lift coefficient bigger. The variation of C_l(rms) can be seen in Fig. 10, Vortex shedding frequency, represented by Strouhal number, St, in thicker boundary layers (lower Reynolds numbers) increases by decreasing G/D and vice versa.

Table 3: 3-D numerical results of flow around circular cylinder far from and near the wall for Re=100

Re=100	G/D=∞	G/D=1	G/D=0.5	G/D=0.2
C_d(mean)	1.269	1.61	1.405	1.165
C_l(rms)	0.111	0.2	0.163	0.598
st	0.161	0.183	0.183*	0.196*
G/δ	-	1.042	0.521	0.208
separation angle	114.72	98.97	95.51	92.29
stagnation angle	0	-2.2	-5.5	-9
Cpb	-0.53	-0.64	-0.52	-0.56

Table 4: 3-D numerical results of flow around circular cylinder far from and near the wall for Re=200

Re=200	G/D=∞	G/D=1	G/D=0.5	G/D=0.2
C_d(mean)	1.208	1.518	1.425	1.143
C_l(rms)	0.306	0.492	0.342	0.417
st	0.192	0.209	0.233	0.25*
G/δ	-	1.19	0.595	0.238
separation angle	108.07	98.97	95.51	92.29
stagnation angle	0	-2.2	-8.1	-11
Cpb	-0.69	-0.86	-0.72	-0.57

Table 5: 3-D numerical results of flow around circular cylinder far from and near the wall for Re=3900

Re=3900	G/D=∞	G/D=1	G/D=0.5	G/D=0.2
C_d(mean)	1.281	1.712	1.544	1.238
C_l(rms)	0.677	1.032	0.896	0.51
st	0.214	0.18	0.233	0.15*
G/δ	-	2.174	1.087	0.435
separation angle	98.98	98.97	92.75	85.5
stagnation angle	0	-2.2	-14.7	-6.8
Cpb	-1.15	-1.71	-1.13	-0.91

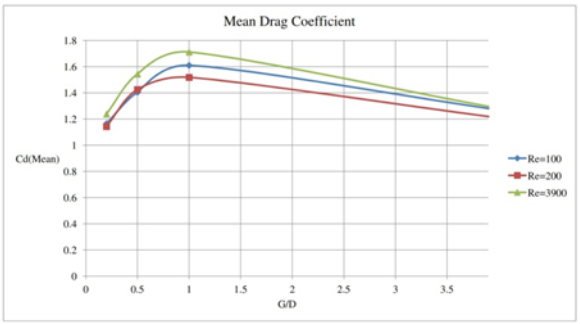

Fig. 9. Mean Drag coefficient versus G/D for Re=100, 200, 3900

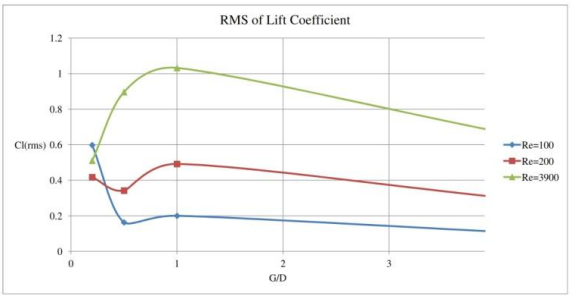

Fig. 10. RMS of lift coefficient versus G/D for Re=100, 200, 3900

Time-averaged horizontal velocity gradient between top and bottom of the cylinder is extracted by two probes and is presented for all cases in table 6 and Fig. 11.

Table 6. Time-averaged horizontal velocity gradient between top and bottom of the cylinder for all cases

G/D	Re=100	Re=200	Re=3900
0.2	0.1065	0.0864	0.2933
0.5	0.0596	0.0469	0.2619
1	0.0836	0.1399	0.3662
∞	0.0012	0.0161	0.0058

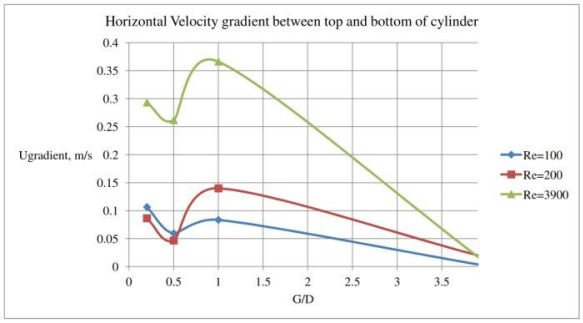

Fig. 11. Time-averaged horizontal velocity gradient between top and bottom of the cylinder versus G/D for Re=100, 200, 3900

The sudden increase in velocity gradient between top and bottom of the cylinder at G/D=1 in all Reynolds numbers is due to the location of bottom probes at the boundary of the wall boundary layer. Intrinsically the

variation of velocity profile at the interference region of the boundary layers becomes considerable.

Vortex shedding suppression can be predicted by monitoring the variations of pressure distribution around the circular cylinder near the boundary, hence suppression can be preceded by modifying the pressure distribution patterns. Vortex shedding suppression observed in 4 cases, all of three cases of flow around a circular cylinder near wall with G/D=0.2 and the other one for flow around a circular cylinder near wall with G/D=0.5 and Re=100. For these cases, a sustained negative pressure is observed at the free-stream side of the cylinder and a less pronounced negative pressure is observed at the wall-side of the cylinder. The maximum of positive pressure coefficient experiences a chamfer in shape and a bit of decrease in value while suppression occurs. Insufficient gradient of pressure between free-stream side and wall-side of cylinder leads to a static and stable state of shear layers, which prevents the process of vortex shedding to proceed or even to form vortex sheets in the high interference conditions of boundary layers, i.e. very low G/δ - the situation that the rolling up of shear layers cannot be happened.

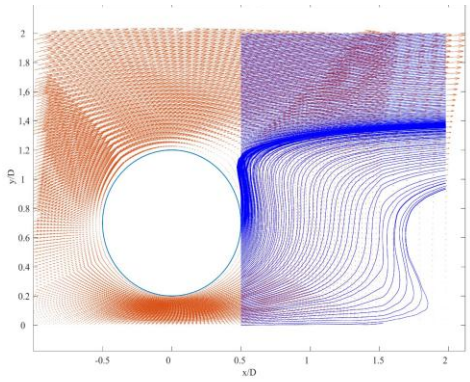

(a)

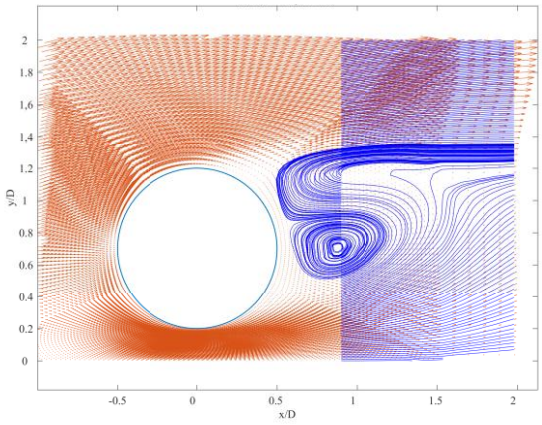

(b)

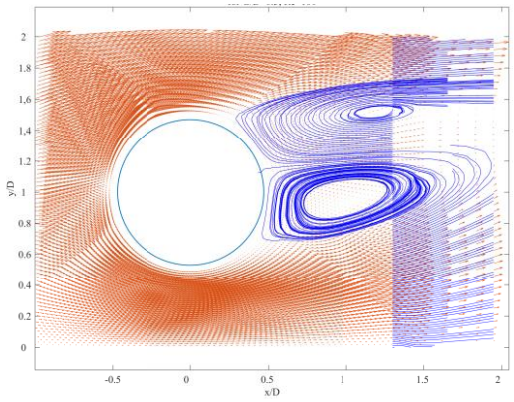

(c)

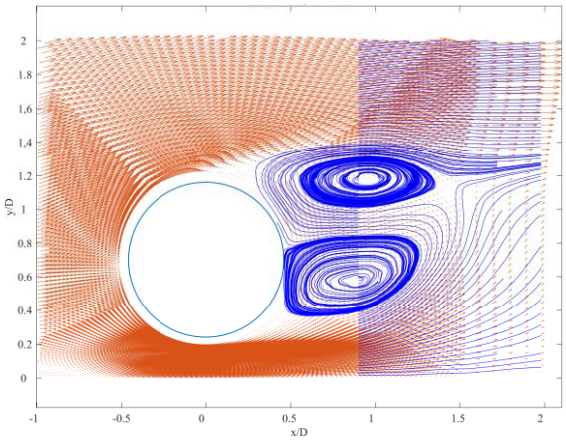

(d)

Fig. 12. Time-averaged streamlines and velocity vectors behind a circular cylinder for (a) G/D=0.2, for Re=100, (b) G/D=0.2, for Re=200, (c) G/D=0.5, for Re=100, (d) G/D=0.2, for Re=3900

Velocity vectors and time-averaged streamlines behind a circular cylinder for the cases subjected to vortex shedding suppression have been demonstrated in Fig. 12.

In order to focus on maintaining or suppression of the vortex shedding process, different aspects of vortex shedding mechanism should be investigated. At subcritical Reynolds numbers Von Karman vortex street is the dominant pattern of vortex shedding which is based on subsequent shedding of swirling vortices from top and bottom of the cylinder. It`s necessary for the vorticity sheets in upper and lower of the wake to be symmetric around the wake centerline and also the upper and lower vortex sheet strengths should be of almost the same range of value to develop vortex shedding in the Von Karman vortex street pattern. The strength of upper and lower vortex sheets can be quantified by circulation or swirling strength value, Γ, which is defined by equation 24:

$$\Gamma = \int\int_{A} \omega_z \, dx dy \tag{24}$$

Where ω_z is the spanwise vorticity and A is the area of the vorticity integration and should be determined for each vortex region. To identify the distinct regions of

vorticity where the vortices can be formed around the cylinder, Q-criterion is employed. The Q-criterion defines a vortex as a connected fluid region with a positive second invariant of the velocity gradient, which means for Q > 0. Q tensor can be defined in terms of strain rate and vorticity tensors by equation 25.

$$Q = \frac{1}{2}\left\|\bar{\Omega}\right\|^2 - \left\|\bar{S}\right\|^2 \tag{25}$$

Where strain rate tensor and vorticity tensor in two dimensions can be expressed as follows in equations 26 and 27:

$$S_{ij} = \frac{1}{2}\left(\frac{\partial u_i}{\partial x_j} + \frac{\partial u_j}{\partial x_i}\right) \tag{26}$$

$$\Omega_{ij} = \frac{1}{2}\left(\frac{\partial u_i}{\partial x_j} - \frac{\partial u_j}{\partial x_i}\right) \tag{27}$$

Time averaged normalized spanwise vorticity contours around the cylinder inside positive Q-criterion regions (colored area) for the cases subjected to vortex shedding suppression have been displayed in Fig. 13.

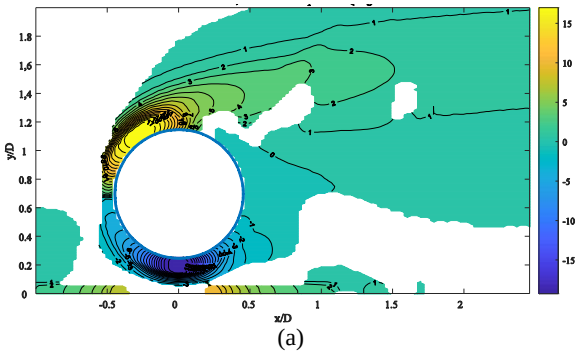

(a)

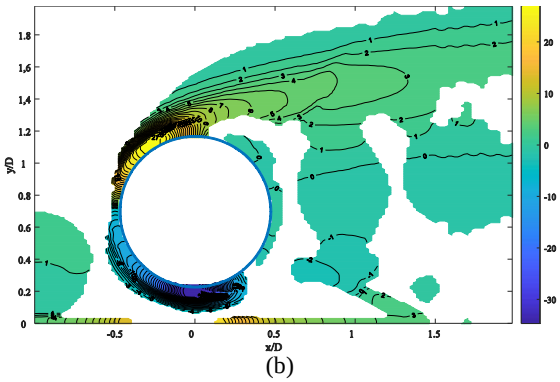

(b)

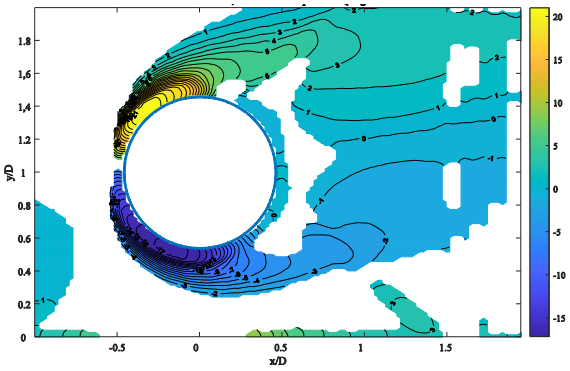

(c)

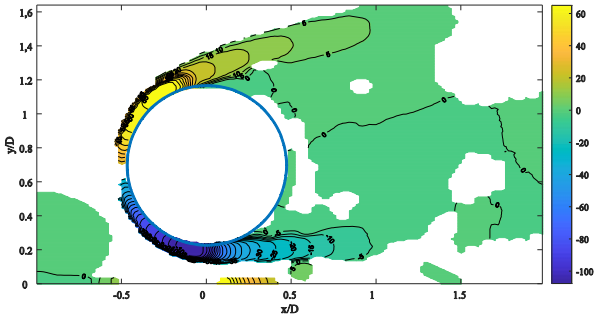

(d)

Fig. 13. Time-averaged normalized spanwise vorticity contours for (a) G/D=0.2, Re=100, (b) G/D=0.2 ,Re=200 (c) for G/D=0.5, Re=100 (d) G/D=0.2, Re=3900 ; colored area denounce the positive Q criterion.

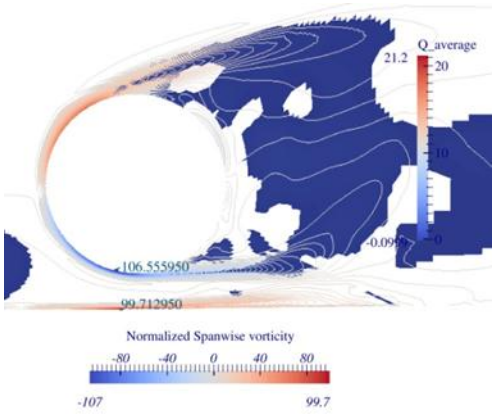

Fig. 14. Time-averaged normalized spanwise vorticity contours and extremum values for G/D=0.2 and Re=3900, colored area denounce the positive Q criterion

Time-averaged normalized spanwise vorticity contours and extreme values for G/D=0.2 and Re=3900 inside vorticity regions is presented in Fig. 14 and shows that the extremums of normalized spanwise in the gap flow between the cylinder and the plane wall contain close values with opposite signs. Which means the vorticity field in the gap flow is supposed to be cancelled out due to the interference of vorticity fields of the cylinder and the wall.

A parameter Λ is introduced as absolute proportion of upper vortex sheet swirling strength to the lower one, which can be a measure of vorticity strength balance between upper and lower vortex sheets. Time-averaged swirling strength for upper and lower vortex

sheets and Λ for all cases is presented in table 7. It can be observed that suppression occurs for the cases with $\Lambda \geq 2$, which implies the unbalance of vorticity content of vortices about the wake centerline. In these cases upper shear layer which feeds into upper vortex gains strength but the lower shear layers weakens and therefore unable to feed vorticity in the vortex region and draw the upper shear layer afterwards.

Table 7. Time-averaged swirling strength for upper and lower vortex sheets and Λ for all cases

		Γl(Lower vortex sheet)	Γu(Upper vortex sheet)	$\Lambda=\lvert \Gamma u/\Gamma l \rvert$
G/D=0.2	Re=100	-0.0014	0.0019	N
	Re=200	-0.000493	0.0013	2.637
	Re=3900	-0.0651	0.1955	3.003
G/D=0.5	Re=100	-0.0013	0.0026	2.000
	Re=200	-0.0018	0.002	1.111
	Re=3900	-0.1224	0.1327	1.084
G/D=1	Re=100	-0.0011	0.0012	1.091
	Re=200	-0.0037	0.0037	1.000
	Re=3900	-0.0687	0.0742	1.080
G/D=∞	Re=100	-0.00147	0.0014	0.952
	Re=200	-0.0044	0.0041	0.932
	Re=3900	-0.0596	0.0601	1.008

Existence of vortical activity and vortex regions do not ensure the maintaining of the vortex shedding mechanism. Vortex shedding mechanism depends on vortex stretching and perturbation growth respectively represented by extensional strain and perturbation vorticity. Rotational field and vortex formation is already discussed by applying Q-criterion and measuring normalized spanwise vorticity contours. According to Sengupta et al. [16] disturbance energy grows while the right-hand side of equation 28 becomes negative which implies a source in energy.

$$\Delta^2 E_d = 2\omega_m.\omega_d + \omega_d.\omega_d - V_m.\nabla\times\omega_d - V_d.\nabla\times\omega_m - V_d.\nabla\times\omega_d \quad (28)$$

Where E_d is the disturbance energy and subscripts "m" and "d" denote mean and disturbance parts of velocity and vorticity fields. This indicates that the last three kinematic terms including velocity and vorticity vectors should contribute as strong source terms to overcome first two terms of vorticity energy dissipation. The mentioned terms can be best represented by the extensional strain. It can be also perceived that the spatial variation of the vorticity field in interaction with the velocity field should contribute to instability in shear layer at the bottom of the cylinder. Extensional strain which can be quantified by the magnitude of strain rate tensor, S, supplies the extension and propagation of the perturbations in the gap flow.

A new parameter called the flow type parameter, λ, is introduced according to the following equation 29:

$$\lambda = \frac{\|S\| - \|\Omega\|}{\|S\| + \|\Omega\|} \quad (29)$$

If λ value approaches -1, it means flow is mostly rotational and if approaches 1, it means planar extensional flow is dominant. Zero value indicates simple shear flow. While extensional strain needs to be large enough to secure vortex stretching in the gap flow, positive λ contours in this region is beneficial and shear layers can feed source generated disturbances from previous cycle of vortex formation. Flow type parameter contours for flow around a circular cylinder for two cases of G/D=0.5 have been compared in Fig. 16. For the first case with Re=100 in which vortex shedding is eventually suppressed, negative dashed contours compactly engages positive contours in the gap flow and interrupts the extensional strain which is dominated by magnitude of strain rate tensor. The flow type parameter contours for the second case with Re=200 is relatively more symmetric with respect to horizontal cylinder centerline and extensional strain is less interrupted by negative contours, which can damp the energy needed to feed the subsequent vortex formation and stretching, Fig. 16.

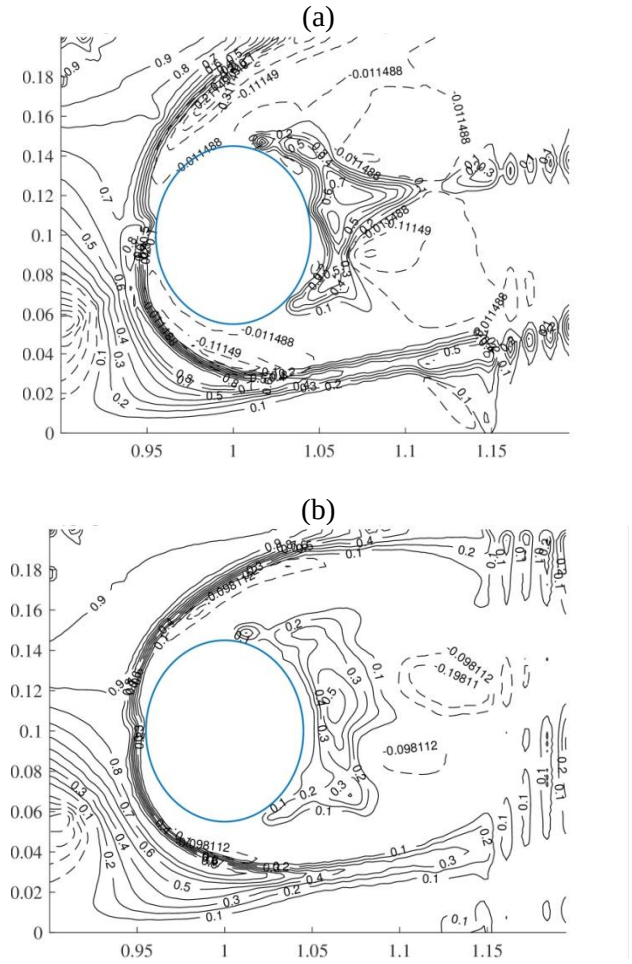

Fig. 16. Time-averaged λ contours around a circular cylinder for (a) G/D=0.5, Re=100, (b) G/D=0.5, Re=200

7. Conclusion

Flow around a circular cylinder near plane has been studied numerically in different flow regimes (Re=100, 200, 3900) with different gap ratios (G/D=∞, 1, 0.5, 0.2). Pressure distribution around the circular cylinder has been utilized to describe the variations in hydrodynamic force coefficients as well as other features of wake flow such as separation and vortex shedding phenomenon near a plane boundary. Plane wall effect on pressure distribution in different flow regimes was also assessed and it was observed that the inception of vortex shedding suppression can be deduced from pressure distribution pattern, through pressure gradient between free-stream-side and wall-side of cylinder and also the sudden decrease in maximum of positive pressure coefficient. Mean drag coefficient increases when cylinder approaches the wall until G/D=1, but when cylinder submerges further in the plane wall's boundary layer, C_d(mean) decreases as C_{pb} decreases. C_l(rms) near the wall in thick boundary layer near the wall, increases as a result of the perturbance of reverse pressure gradient above and below the cylinder which makes the positive fluctuations of lift coefficient bigger. In a constant flow regime, upper separation point moves upward by decreasing G/D, indicating that the separation angle, θ_s decreases too. This can be described by the growing stream-wise pressure gradient induced by the gap flow.

Vortex shedding suppression can also be assessed by the means of quantitative measures obtained from velocity and vorticity fields. A parameter Λ, the ratio of swirling strength of the upper vortex sheet to the lower one, has been introduced to detect the occurrence of vortex shedding suppression. Vortex shedding suppression is observed for the cases with the high unbalance vorticity content in the vortex regions, namely for $\Lambda \geq 2$. To ensure the evolution and stretching of vortices in the gap flow, the state of extensional strain is explored in the gap flow via the flow type parameter, λ. It has been observed that the presence of negative contours of λ in the gap flow acts as a sink of energy and interrupts vortex stretching at the lower side of the cylinder, which consequently can lead to the vortex shedding suppression.

8. References

1- Batham, J.P., (1973). *Pressure distributions on circular cylinders at critical Reynolds numbers*. Journal of Fluid Mechanics, Vol.57, p.209–228

2- Bearman P.W. & Zdravkovich M.M., (1978). *Flow around a circular cylinder near a plane surface*, Journal of Fluid Mechanics, Vol.89, p.33-47.

3- Zdravkovich M.M., (1985). *Forces on a circular cylinder near a plane wall*, Applied Ocean Research Vol.7, p.197-201.

4- Buresti, G., and Lanciotti, A., (1992). *Mean and fluctuating forces on a circular cylinder in cross-flow near a plane surface*, Journal of Wind Engineering and Industrial Aerodynamics, Vol.41(1–3), p.639–650.

5- Oner, A.A., Kirkgoz, M.S., Akoz, S., (2008). *Interaction of a current with a circular cylinder near a rigid bed*, Journal of Ocean Engineering, Vol.35, p.1492-1504.

6- Lei C., Cheng L., Kavanagh K., (1999). *Re-examination of the effect of a plane boundary on force and vortex shedding of a circular cylinder*, Journal of Wind Engineering and Industrial Aerodynamics, Vol.80(3), p.163–286.

7- Price, S.J., Sumner, D., Smith, J.G., Leong, K., Paidoussis, M.P., (2002). *Flow visualization around a circular cylinder near to a plane wall*, Journal of Fluids and Structures Vol.16, p.175–191.

8- Wang, X. K., Tan, S. K., (2008). *Near-wake flow characteristics of a circular cylinder close to a wall*, Journal of Fluids and Structures, Vol.24(5), p.605–627.

9- Lin W. J., Lin C., Hsieh S. C, Dey S., (2009). *Flow characteristics around a circular cylinder placed horizontally above a plane boundary*, Journal of Engineering Mechanics, Vol.135, p.697-716.

10- Dipankar, A., Sengupta, T. K. (2005). *Flow past a circular cylinder in the vicinity of a plane wall*, Journal of Fluids and Structures, Vol.20(3), p.403–423.

11- Sarkar, S., Sarkar, S. (2010). *Vortex dynamics of a cylinder wake in proximity to a wall*, Journal of Fluids and Structures Vol.26(1), p.19–40.

12- He, G. S., Wang, J. J., Pan, C., Feng, L. H., Gao, Q., Rinoshika, A,. (2017). *Vortex dynamics for flow over a circular cylinder in proximity to a wall*, Journal of Fluid Mechanics. Vol.812, p.698–720.

13- Menter F. R., (1994). *Two-equation eddy-viscosity turbulence models for engineering applications*. AIAA Journal, Vol.32(8), p.1598–605.

14- Schlichting, H., Gersten, K. (2017). *Boundary-Layer Theory*. Springer, Heidelberg.

15- Cao, H., Wan, D., (2010). *Application of OpenFOAM to Simulate Three-Dimensional Flows past a Single and Two Tandem Circular Cylinders*, Proceedings of the Twentieth International Offshore and Polar Engineering Conference Beijing, China, June 20-25, 2010.

16- Sengupta, T.K., De, S., Sarkar, S., (2003). *Vortex-induced instability of incompressible wall-bounded shear layer*. Journal of Fluid Mechanics Vol.493, p.277–286.